



Bubble nucleation, growth and surface temperature oscillations on a rapidly heated microscale surface immersed in a bulk subcooled but locally superheated liquid under partial vacuum

Richard E. Cavicchi^a, C. Thomas Avedisian^{b,*}

^a Process Measurements Division, National Institute of Standards and Technology, Gaithersburg, MD 20899, United States

^b Sibley School of Mechanical and Aerospace Engineering, Cornell University, Ithaca, NY 14853-7501, United States

ARTICLE INFO

Article history:

Received 10 May 2011

Received in revised form 30 June 2011

Accepted 30 June 2011

Available online 27 August 2011

Keywords:

Boiling

Superheated liquid

Homogeneous nucleation

Bubble nucleation

Surface tension

Bubble growth

Condensation

Temperature oscillations

ABSTRACT

The effect of ambient pressures below atmospheric, liquid subcooling and heating rate on bubble dynamics associated with rapid evaporation in highly superheated water is investigated. Platinum films of various aspect ratios are electrically heated under partial vacuum and the average metal film temperature monitored during a power pulse of duration of several tens of microseconds.

At high liquid subcooling, the surface temperature of the pulse-heated thin platinum strips is shown to oscillate with a frequency on the order of 0.5 MHz. The oscillation frequency increases with ambient pressure in the range 0.02 MPa and 0.101 MPa, and decreases with increasing ambient temperature at a fixed pressure. An unusual dynamic instability is observed in which the surface temperature is constant before relaxing into oscillations, and the delay to oscillations increases with decreasing pressure.

High speed imaging shows that the bubble growth phase of the oscillation is associated with surface heating and the collapse phase with surface cooling in the cyclic temperature history. These effects are explained by a bubble growth theory that includes a heat loss mechanism to the surrounding liquid. The nucleation temperature is unaffected by pressure in the sub-atmospheric range examined and it approaches the theoretical superheat limit for water at a heating rate of about 10^9 °C/s.

© 2011 Elsevier Ltd. All rights reserved.

1. Introduction

Bubble nucleation and growth on microscale surfaces¹ immersed in sub-cooled liquids is an important process in applications that use bubble formation as a means to push fluid through microscale structures, as in thermal ink jet printing [2,3] and bubble pump designs [4–6]. Many parameters influence the phase change dynamics on microscale surfaces including gravity, liquid subcooling, and heater size [1,7,8] and pressure. Under some conditions the surface temperature can oscillate during the phase change process. Observed in the post-nucleation regime, oscillations have been noted for 65 μm square thin metal films immersed in water and aqueous methanol mixtures [9,10], 100 μm diameter by 4 cm long platinum wires in organic fluids [11] and for sub-microscale surfaces [12] under atmospheric pressure conditions. The existence

of oscillations may signal an erratic bubble dynamic that influences the quality of the droplet ejection process and is therefore important to understand.

With reference to Fig. 1, five periods characterize the overall processes leading up to surface temperature oscillations for a microscale surface with a sustained constant heat input: an initial surface heating profile (1) that consists of a somewhat exponential form associated with liquid heating; a transition period (2) marked by an inflection point in the evolution of average surface temperature that signifies the state where a bubble is nucleated; a period similar to the first (3) but with an initially higher heating rate because heat transfer is now across a vapor layer (with lower thermal conductivity compared to the liquid) because the nucleated bubble expands laterally over the surface; and remaining periods where the surface temperature is constant (4) followed by an oscillatory period (5) that can sustain itself indefinitely for a constant heat input.

The present investigation is undertaken to further examine the surface temperature oscillation phenomenon and conditions that affect it. In particular, the influence of surface heating rate, ambient pressures below atmospheric, and bulk liquid subcooling are considered for heating times on the order of several tens of microseconds. By imposing sub-atmospheric pressure conditions the

* Corresponding author. Tel.: +1 607 592 7915; fax: +1 607 255 1222.

E-mail address: cta2@cornell.edu (C. Thomas Avedisian).

¹ A microscale surface is one for which the characteristic length of the heater, L , is much smaller than the Taylor wavelength [1] $L_{\text{Tay}} = \sqrt{\frac{\sigma}{g(\rho_l - \rho_g)}}$. For water at 403 K (the reference temperature at which properties in Table 1 are evaluated in the present study), $L_{\text{Tay}} \approx 2$ mm, though heaters with much smaller L (order of less than 100 μm) are used in this study.

Nomenclature

AR	aspect ratio of heater (length divided by width)	t_w	waiting time
C_p	Pt film specific heat ($\text{J kg}^{-1} \text{K}^{-1}$)	t_L	time for a bubble to reach size R_{ca} (s)
g	acceleration due to gravity (m/s^2)	T	Platinum temperature ($^{\circ}\text{C}$)
k_L	liquid thermal conductivity ($\text{W m}^{-1} \text{ }^{\circ}\text{C}^{-1}$)	T_{∞}	ambient fluid temperature ($^{\circ}\text{C}$)
k_s	solid thermal conductivity ($\text{W m}^{-1} \text{ }^{\circ}\text{C}^{-1}$)	T_{nuc}	bubble nucleation temperature ($^{\circ}\text{C}$)
L	length of heater (m)	T_w	surface temperature ($^{\circ}\text{C}$)
N_s	number density of molecules at the surface (molecules/ m^2)	V_{in}	input voltage to bridge (V)
N_o	number density of molecules in the bulk (molecules/ m^3)	V_o	voltage amplitude for pulse input (V)
p_{in}	input power (W)	\underline{V}_{out}	bridge output voltage (V)
p_o	input power (W) for square pulse		
P_o	ambient pressure	Greek letters	
P_{sat}	pressure inside the bubble	α	thermal diffusivity ($\text{m}^2 \text{ s}^{-1}$)
R_c	critical bubble radius	δ	separation of the equimolar surface from the surface of tension (m)
R	bubble radius	θ	contact angle
R_1	fixed wheatstone bridge resistor (Ω)	γ	voltage ramp rate (V/s)
R_2	fixed wheatstone bridge resistor (Ω)	ρ_L	density liquid (kg m^{-3})
R_3	adjustable resistor (Ω)	ρ_g	density gas (kg m^{-3})
R_H	heater resistance (Ω)	ρ_s	density of metal film (kg m^{-3})
R_L	lead resistance due to electrical connections (Ω)	σ	surface tension
R_T	$R_L + R_H$ (Ω)	τ	$\equiv t_b/t_w$
R_{∞}	heater resistance at $T_{\infty} = 22^{\circ}\text{C}$	v	volume of Pt film (m^3)
S	conduction shape factor (m)		
t	time (s)		
t_b	bubble growth time		

nucleation temperature will be constant. In saturated or superheated liquids, bubbles should always grow and not collapse and temperature oscillations should not occur. Thin metal films of high aspect ratio (AR) are employed to promote uniform surface temperatures during power pulses so that bulk subcooling will provide the primary mechanism for the collapse process that leads to surface quenching and an oscillating temperature history.

Water is selected as the working fluid because of the extensive property database available for it and familiarity with related experiments of rapid evaporation at the superheat limit [9,10,13–16]. Since surface temperature oscillations are speculated to track with bubble growth and collapse cycles as suggested by the schematics of Fig 1b and c, some visualizations of bubble morphology are also included using a laser flash method described previously [13]. For these visualizations, ethanol proved to have a more repeatable bubble morphology for the long pulse times investigated compared to water so some results on bubble dynamics are shown for ethanol and correlated to the temperature cycle.

2. Experiment

The heaters employed in the present investigation are layered structures consisting of a 300 μm thick Si wafer substrate, a 200 nm thick SiO_2 insulating layer, a 30-nm-thick titanium adhesion layer and a 200 nm thick Pt film on which the boiling process occurred. Fig. 2 is a cross-sectional schematic of the heater structure. Experiments were carried on platinum (Pt) films fabricated into several different ARs to facilitate measurements of the inflection point, delay time and oscillation frequency and photographing bubble shapes by high speed imaging. No single AR could allow for all such information.

Three ARs were examined. A 3 $\mu\text{m} \times 200 \mu\text{m}$ (AR = 67) Pt film was used for measurements of T_{nuc} because temperature is uniform along the length of such films. This device is essentially the same as used in a previous study [14]. Fig. 3 shows a photomicrograph of a representative heater. High AR films are not suitable for

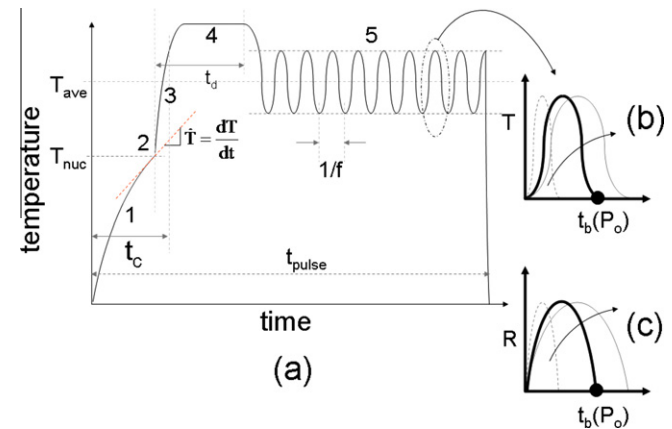


Fig. 1. (a) Illustration of temperature history for a pulse-heated microheater showing the stages prior to temperature oscillations. (b) Representation of one cycle of a temperature oscillation. (c) Suggested correspondence of one bubble growth and collapse cycle with a temperature cycle. Arrows in (b) and (c) show decreasing P_o or increasing T_{∞} .

temperature oscillation studies because different boiling modes can co-exist over long surfaces, as shown in some visualizations of explosive bubble growth on 1.91 cm by 3.81 cm gold films in R-113 ($\text{CCl}_2\text{FCClF}_2$) [17]. Reducing the heater area appears to make the bubble morphology slightly more uniform by confining the bubble to a smaller footprint, which also facilitates photographing the bubble during its growth/collapse cycle. A 4 $\mu\text{m} \times 40 \mu\text{m}$ (AR = 10) Pt film and a 7 $\mu\text{m} \times 46 \mu\text{m}$ (AR = 6.6) Pt film were used for recording surface temperature oscillations and for photographing bubbles, respectively. Voltage pulses ranged from 30 μs to 90 μs for the detailed observations reported here.

The metal films were heated by passing a current through them. The films formed one leg of a Wheatstone bridge circuit as illustrated in Fig. 4. The arrangement is similar to that described previously [14]. The bridge consists of the Pt film heater (resistance

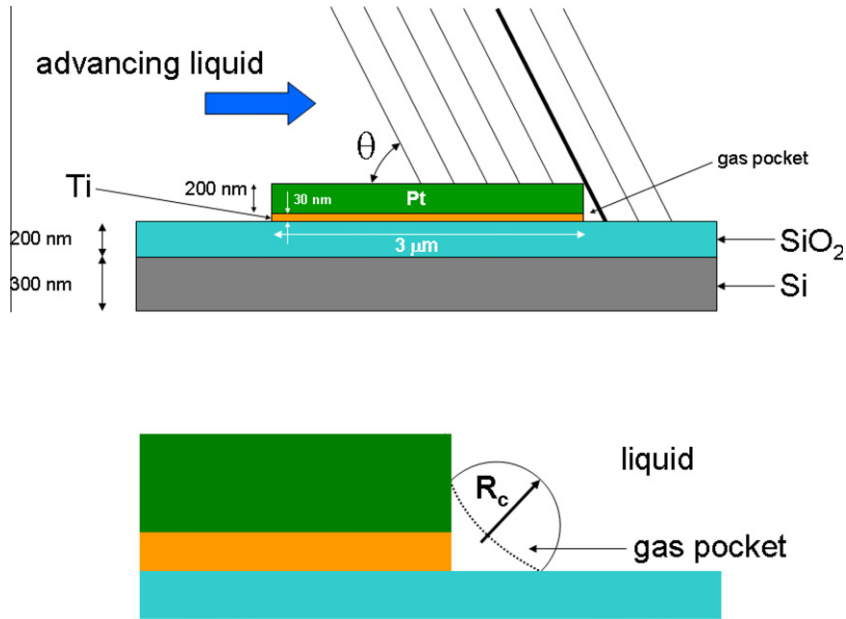


Fig. 2. Cross section of the thin film structures (not to scale). Also shown is a potential mechanism for trapping a gas pocket in the corner of the raised metal film as the liquid with advancing contact angle θ spreads over the surface.

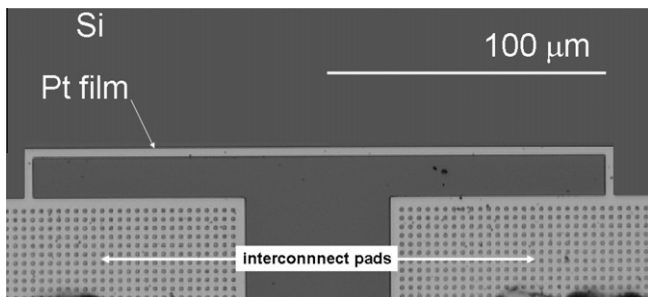


Fig. 3. Photomicrograph (top view) of an AR = 67 platinum heater. Light area Pt and dark area is Si.

of R_H) in series with a lead resistance R_L due to the electrical connections. The Si chip with platinum metallization is glued into a dual-in-line (DIP) package. Gold wire bonds provide electrical connections to the instrumentation. A potentiometer on the opposite leg of the bridge (R_3) allows for balancing the bridge. The DIP is placed in a vacuum chamber with electrical connections provided by vacuum feed-throughs. Pressures ranging from 0.02 MPa to 0.101 MPa, as measured by a capacitance manometer gauge, were studied. The lower limit was still large enough that water would not immediately evaporate when exposed to a partial vacuum of this level.

Input power was provided by signal generators capable of producing a time dependent input voltage, $V_{in} = V_o + \gamma t$, as either a

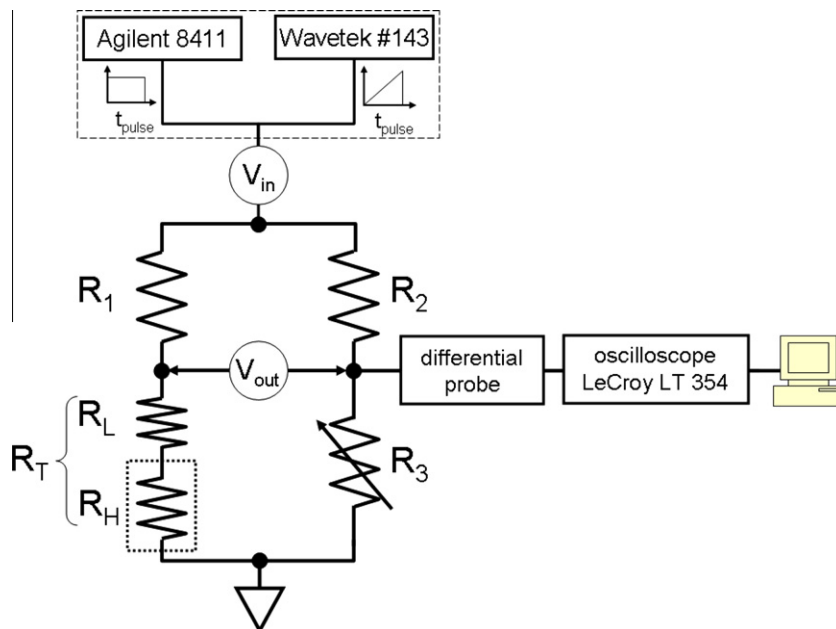


Fig. 4. Schematic of bridge circuit. The dotted box is a pressure chamber.

square wave input voltage $V_{in} = V_o$ ($\gamma = 0$ by an Agilent 8411 pulse generator²), or a linear ramped $V_{in} = \gamma t$ ($V_o = 0$ by a Wavetek #143, 20 MHz, signal generator). These two forms served several purposes. The ramp input facilitated a gradual surface temperature increase and more precise control of the heating rate at the nucleation temperature. A pulse input allowed for higher heating rates before bubble nucleation, though with less control of the heating rate at the inflection point. The data were stored on a PC interfaced with a digital oscilloscope (LeCroy LT354) through LabView control to record the evolution of V_{out} .

For a balanced bridge ($R_1 = R_2, R_3 = R_T$) input power p_{in} is related to V_{in} as

$$p_{int}(t) = V_{in}^2(t) \frac{R_T}{(R_1 + R_T)^2} \quad (1)$$

where R_H is related to R_T as $R_H = R_T - R_L$. The lithography to fabricate the AR = 10 heaters included metal lines that connected to the smaller heater. These lines contributed a significant lead resistance, $R_L = 21.0 \Omega$. This correction to R_T was necessary to convert R_H to temperature for this film. The metalized pattern for the AR = 66.7 film consisted of the long heater directly connected to the wire bond pad, essentially making $R_L \ll R_T$ for this aspect ratio.

R_H was calibrated by measuring its electrical resistance as a function of temperature in a temperature-controlled furnace. The results are correlated as

$$R_H = R_\infty (1 + \xi(T_H - T_\infty)) \quad (2)$$

where R_∞ is the platinum film resistance at $T_\infty = 22^\circ\text{C}$ and ξ is the coefficient of thermal resistance (CTR). For the AR = 67 film, $\xi \approx 0.0025^\circ\text{C}^{-1}$ [14] and for the AR = 10 film $\xi \approx 0.0018^\circ\text{C}^{-1}$. The difference in these CTRs is the result of annealing the AR = 67 film during fabrication, while no annealing was done for the AR = 10 film. For the AR = 67 film $R_1 = R_2 = 38.33 \Omega$ was used in the bridge, and $R_\infty = 51.16 \Omega$. For the AR = 10 film, $R_1 = R_2 = 56.0 \Omega$ was used in the bridge and $R_\infty = 38.0 \Omega$.

Experiments were carried out to show the variation of nucleation temperature with heating rate on the AR = 66.7 films as they provide a more uniform temperature and therefore a more accurate nucleation temperature. The heating rates ranged from 10^3°C/s to 10^8°C/s for the ramp input, and from 10^7°C/s to 10^9°C/s for the pulse V_{in} . For the square pulse, the form of $p_{in}(t)$ follows $V_{in}(t)$ within about 13% over temperatures ranging from 22°C to 300°C for the AR = 67 film and within about 4% for the AR = 10 film. Experiments were carried out using deionized high-resistivity 18 M Ω -cm water, which covered the Pt heater during the voltage pulse. A 500 μL drop of water flooded the surface of each chip during an experiment.

Some limited visualizations of the evolution of bubble morphology were obtained on the AR = 6.6 platinum film during a power pulse using a high-speed laser-flash method [13]. This information determines the extent to which growth/collapse cycles qualitatively track with surface temperature oscillations. The ability to obtain this correlation by microphotography that captures one image per pulse is somewhat problematic when the bubble dynamic does not have especially good stability and repeatability at each instant. Water was problematic in this regard for the long power pulses examined in the present study, on the order of tens of microseconds (whereas for short pulses, on the order of a few μs , bubbles forming in superheated water by rapid evaporation showed good repeatability [15,16]). Bubble formation in superheated ethanol showed much less pulse-to-pulse variations than

water though there was still some variability from pulse to pulse for a fixed delay after the start of a pulse. Accordingly, time-lapsed sequences of bubble growth and collapse in ethanol are used to show the extent to which the growth/collapse cycle tracks with surface temperature.

3. Results and discussion

Fig. 5 shows representative data for the evolution of average surface temperature for a 2 μs square pulse (Fig. 5a) and a 275 μs ramped pulse (Fig. 5) at 0.101 MPa. The input for both pulses was adjusted so that the inflection points signifying nucleation occurred near the end of the pulse. For the pulse input ($\gamma = 0, V_o \neq 0$, Fig. 5a) the evolution of average platinum surface temperature is such that $\frac{dT}{dt}|_{t=0} > 0$ and $\frac{d^2T}{dt^2}|_{t \geq 0} < 0$ while for the ramp input ($V_o = 0, \gamma \neq 0$, Fig. 5b), $\frac{dT}{dt}|_{t=0} = 0$ and $\frac{d^2T}{dt^2}|_{t \geq 0} > 0$. These trends are explained as follows.

Taking the finite-sized metal film at the interface between two semi-infinite media, assuming that the temperature distribution in each region (solid and liquid) instantaneously adjusts to changes in the film temperature, that the pulse duration is short enough that conduction in the fluid is the only mode of heat transfer, designating “S” as a suitable shape factor for conduction from the film to the solid and liquid on either side of it, that a spatially uniform heat generation in the metal film occurs (with p_{in} from Eq. 1 and $V_{in} = V_o + \gamma t$) and taking $\Psi \equiv \frac{R_T}{(R_1 + R_T)^2}$ as approximately constant for this analysis, the temperature of the metal patch modeled as a lumped thermal system is

$$T = T_\infty + \frac{\Psi V_o^2}{S(k_L + k_s)} \left((1 - e^{-\beta t}) + 2 \frac{\gamma}{\beta V_o} (\beta t - (1 - e^{-\beta t})) \right) + 2 \left(\frac{\gamma}{\beta V_o} \right)^2 (\beta t (\frac{1}{2} \beta t - 1) + (1 - e^{-\beta t})) \quad (3)$$

where

$$\beta = \frac{S(k_L + k_s)}{v \rho C_p} \quad (4)$$

From this simple model, the two cases covered in Fig. 5 – $V_{in} = V_o$ (Fig. 5a for $\gamma = 0$) and $V_{in} = \gamma t$ (Fig. 5b for $V_o = 0$) – are consistent with Eq. (3) for both the initial derivatives and curvatures. For long pulse durations ($t \rightarrow \infty$), Eq. (3) shows that T approaches a constant for $V_{in} = V_o$ while $T_\infty t^2$ for $V_{in} = \gamma t$. Though the pulse durations depicted in Fig. 5 are too short to fully confirm these trends, the data qualitatively suggest them to be consistent with these limits.

For constant V_{in} (Fig. 5a) an inflection point is evident at about 1.7 μs into the heating pulse at 265°C . The inflection point signifies incipient bubble nucleation. For the ramped power input (Fig. 5b) a lower nucleation temperature (approximately 205°C) at 240 μs is found due to the lower heating rate. While these inflection point temperatures show significant superheating of water by over 100°C , they are far below the homogeneous nucleation temperature for water [18].

Fig. 6 shows the effect of heating rate on inflection point temperature at atmospheric pressure (the heating rate was estimated by linearizing the evolution of temperature from the initial state to the inflection point). Data for both ramp and pulse inputs are shown. The ramp input facilitated low heating rates (less than 10^6°C/s) while square pulses allowed heating rates up to about 10^9°C/s to be achieved. Between 10^7°C/s and 10^8°C/s the pulse and ramp inputs yielded essentially the same nucleation temperature showing the consistency of the two methods for heating the films.

The nucleation temperature is essentially constant at about 200°C below a heating rate of about 10^6°C/s and increases at higher rates. This temperature is higher than the 180°C average temperature measured by Li and Peterson [19] for degassed water on

² Certain commercial instruments are identified to adequately specify the experimental procedure. In no case does such identification imply endorsement by the National Institute of Standards and Technology. This statement applies to all instruments mentioned in this article.

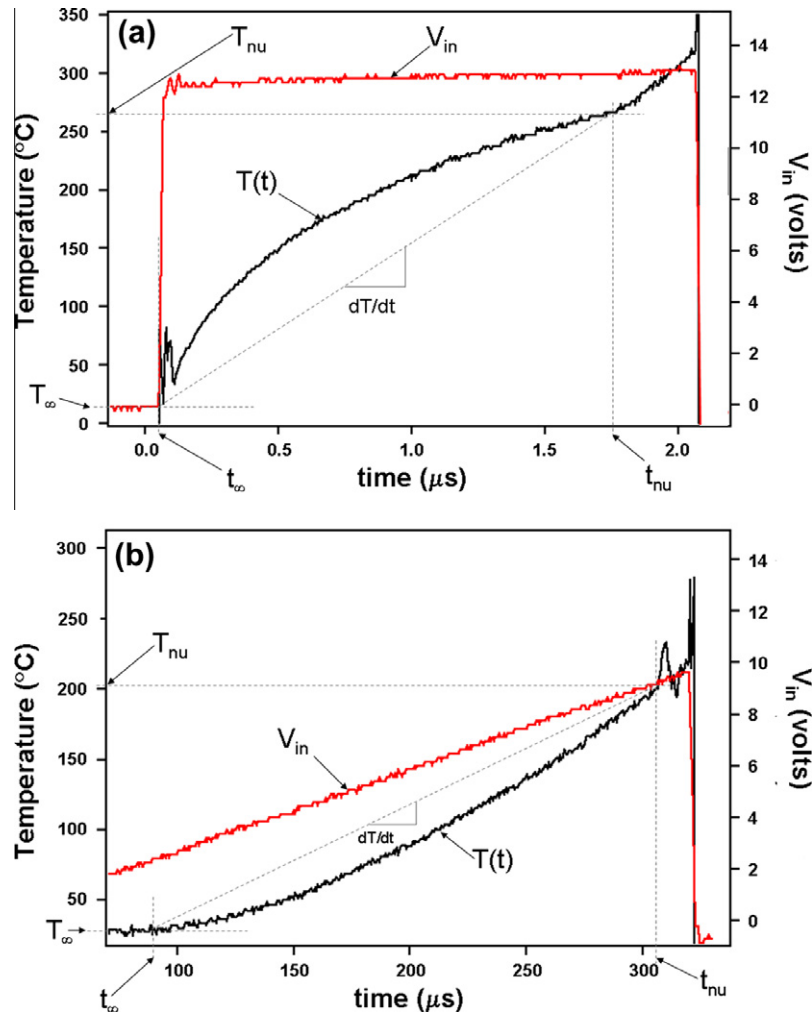


Fig. 5. Influence of input waveform on average film temperature: (a) pulse input, $V_{in} = 12.9$ V; (b) ramp input. V_{out} is converted to temperature which is along the left axis while the right axis shows the form of V_{in} .

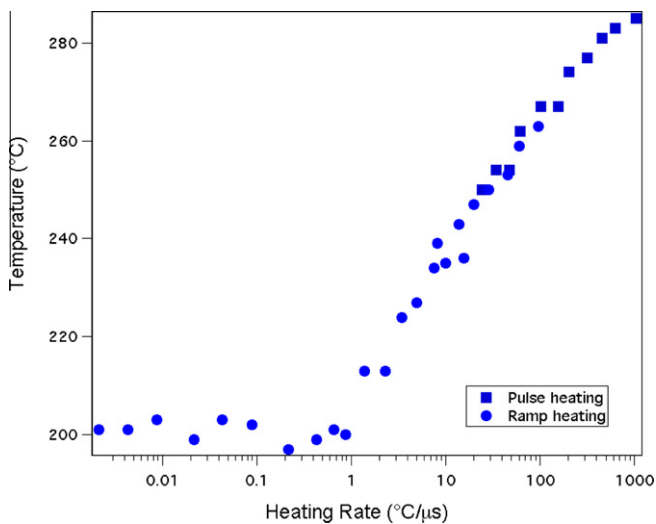


Fig. 6. Nucleation temperature as a function of heating rate. The heating rate was approximated as in Fig. 5.

100 μm square films ($AR = 1$). Nucleation was noted to be initiated in the central portion of the films where a conduction analysis showed the temperature to be 205 $^{\circ}\text{C}$, thus suggesting significant temperature gradients over the surface. The $AR = 67$ platinum film

used in the present study for measuring the nucleation temperature should have a negligible temperature distribution along the 100 μm length and provide a more accurate incipient boiling temperature for low heating rates.

Two processes can trigger bubble nucleation: random density fluctuations; and nucleation of pre-existing gas pockets that form by the process of immersing the film in water. For the latter situation, “nucleation” would denote the process of a gas pocket stabilizing at the advancing contact angle and then growing to macroscopic size.

The nucleation temperature of 200 $^{\circ}\text{C}$ is too low for density fluctuations to be a relevant mechanism for a phase transition over the pressure range investigated. On a microscopically smooth surface the bubble shape will be some variant of a truncated sphere depending on the contact angle in the liquid and geometry of the surface. The energy to form a bubble at the surface will be lower than for a spherical bubble but the number density of molecules at the surface (N_s , molecules/ m^2), which may be considered as potential nucleation “sites”, is lower than in the bulk (N_o , molecules/ m^3) with $N_s \sim N_o^{2/3}$ [20] so that the probability of homogeneous nucleation at a surface could conceivably be lower than in the bulk for a liquid in contact with a solid. The contact angle for water on most metals is low, generally below about 50 $^{\circ}$ [21] so that the energy barrier for a flat smooth surface is close to the bulk value. As such, homogeneous nucleation in the bulk does not appear to be favored at the low heating rates in Fig. 6. This leaves the

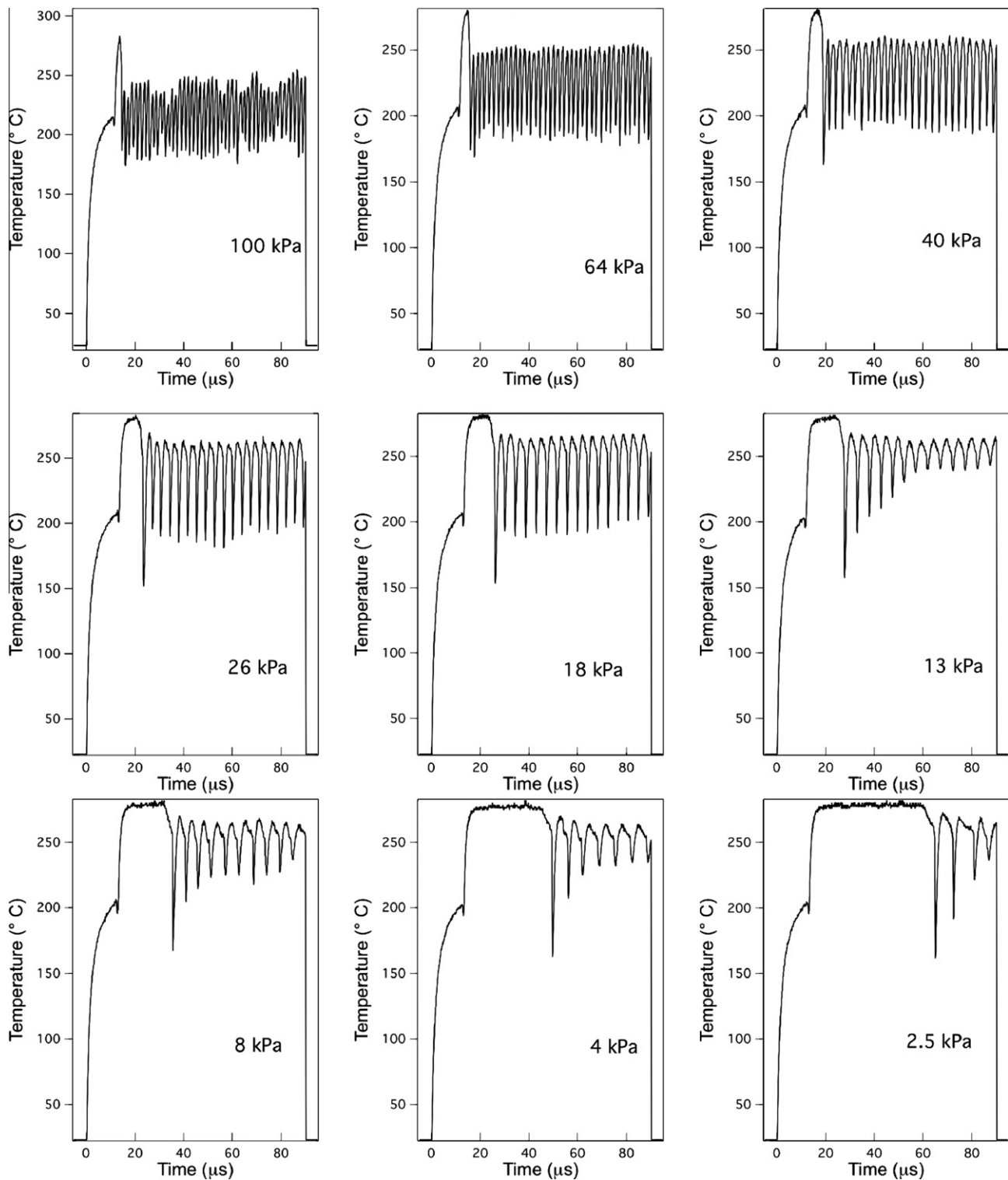


Fig. 7. Effect of ambient pressure on the evolution of surface temperatures for 90 μs pulse widths showing features that roughly correspond to Fig. 1. Pressure is given in the inset to the figures. Applied pulse voltage was 6.6 V. Device aspect ratio AR = 10.

prospect that pre-existing nuclei or gas pockets could trigger bubble nucleation at heating rates below 10^6 $^{\circ}\text{C}/\text{s}$.

A mechanism to create gas pockets at surfaces comes from ideas developed by Lorenz et al. [22]. An advancing liquid front on a surface can trap air as the front moves past surface imperfections. Though the microheaters used in the present study are microscopically smooth, they are raised structures with a height of about

230 nm. The corner could serve as a sort of surface imperfection that traps gas as depicted in Fig. 2. When the films are immersed in water, liquid floods the surface and spreads over it with an advancing contact angle θ as shown in Fig. 2 (the corners are not as sharp as depicted in Fig. 2 but have a more rounded shape). Gas pockets could become trapped after full immersion. The effect of bubble nucleation at the corners of intersecting surfaces was

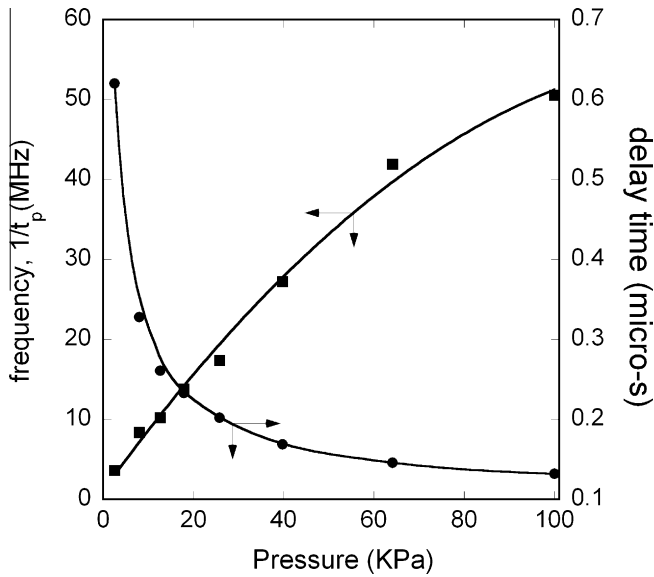


Fig. 8. Variation of frequency (filled squares) and delay time (filled circles) for the first oscillation cycle with ambient pressure.

also noted in a previous study [23] though in that study density fluctuations were considered as the mechanism for bubble nucleation.

Nucleation of a gas pocket requires achieving a state of static mechanical equilibrium for a critical size bubble that would then begin to grow. For such a bubble,

$$P_{\text{sat}}(T_w) - P_o = \frac{2\sigma(T_w, R_c)}{R_c} \quad (5)$$

where it is assumed that $P_{\text{sat}}(T)$ is the pressure inside a bubble of radius R_c . The surface tension is related to bubble radius as [24]

$$\sigma = \frac{\sigma_\infty}{1 + \frac{\delta(R_c)}{R_c}}, \quad (6)$$

where δ represents the separation of the equimolar surface from the surface of tension. In the general case it depends on bubble size. A recent study developed numerical predictions for δ in terms of radius [25]. From this work and over the range of temperatures of interest in this study, which is between the boiling point of water (373 K) and the superheat limit (approximately 573 K at atmospheric pressure), the water surface tension is found to be essentially the bulk value, $\delta/R_c \ll 1$. At 200 °C (473 K), $\sigma \approx 0.037$ N/m [1] and $P_{\text{sat}} \approx 1.56$ MPa [26] so that from Eq. (5) $R_c \approx 51$ nm for $P_o = 0.101$ MPa. Given that the thickness of the Pt/Ti layer is 230 nm, it is conceivable that a 51 nm diameter gas pocket could be formed when the platinum films are immersed in water as suggested in Fig. 2. A critical size bubble of fixed radius would keep the nucleation temperature relatively constant.

With increasing heating rates, density fluctuation processes appear to exert an ever-increasing influence over the nucleation temperature. At the highest rates in Fig. 6 the homogeneous nucleation temperature for water is approached, even though a gas pocket may already exist at the surface. In this event, bubble nucleation would become a sort of hybrid process influenced by gas pockets and density fluctuations with density fluctuations controlling at the highest heating rates. The matter to consider concerns the relative times to form a bubble of a given size and the time for the surface to reach high temperatures where the probability for homogeneous nucleation is appreciable.

From classical bubble growth theory for heat transfer controlled growth, $R \sim C_1 t^{1/2}$ [27,28] where C_1 depends on thermal properties

($C_1 \sim \text{m/s}^{1/2}$). The time for a bubble to reach a characteristic size $R = R_{ca}$ (without departing) after it starts growing will therefore scale as $t_L \sim (\frac{R_{ca}}{C_1})^2$. For heating at a constant rate (ξ) that begins at $T = T_\infty$ and ends when $T = T_{\text{nuc}}$, $\xi \sim \frac{T_{\text{nuc}} - T_\infty}{t_{\text{nuc}}}$. The liquid will be heated to the nucleation temperature even if gas pockets (pre-existing bubbles) are present if $t_{\text{nuc}} \ll t_L$ or $\xi \gg (T_{\text{nuc}} - T_\infty)(\frac{C_1}{R_{ca}})^2$. In this case, the liquid is being heated while a bubble is growing on it but the bubble growth process is too slow to prevent the liquid from being significantly superheated. This is the situation believed to be responsible for the platinum film heaters examined in the present study being capable of approaching the homogeneous nucleation temperature at the highest heating rates while water is in contact with the surface. At low heating rates, $\xi \ll (T_{\text{nuc}} - T_o)(\frac{C_1}{R_{ca}})^2$ and the surface is not heated fast enough before a bubble grows to cover the surface.

Once nucleation occurs, the response of the surface temperature to bubble nucleation and growth is shown in Fig. 7 for pulse durations of 90 μs . The overall form of the variation of temperature qualitatively corresponds to the schematic of Fig. 1. Interestingly, immediately after the inflection point the temperature is observed to drop slightly, and then quickly recover. This effect may be related to the nucleated bubble rapidly growing over the surface and the vapor temperature momentarily dropping as the bubble absorbs latent heat.

The inflection point temperatures in Fig. 8 are essentially unchanged as the pressure is reduced. This result would be consistent with homogeneous nucleation theory [18] whereby $T_{\text{nuc}} \approx C_2 \frac{\sigma^3}{(P_{\text{sat}}(T_{\text{nuc}}) - P_o)^2}$. C_2 is a constant that depends on, among other variables, the nucleation rate. Because $P_{\text{sat}}(200 \text{ °C}) \approx 1.48$ MPa and $P_o < 0.101$ MPa, then $P_{\text{sat}} \gg P_o$ thus making T_{nuc} virtually independent of P_o for subatmospheric pressures.

As shown in Fig. 7, a delay period ensues after nucleation before temperature oscillations begin. This period increases as P_o decreases. Fig. 8, derived from the data in Fig. 7, further shows this trend. Heat loss from the bubble surface to the ambience is proportional to $\Delta T = T_{\text{sat}}(P_o) - T_\infty$. For fixed T_∞ , ΔT decreases as P_o decreases (because $T_{\text{sat}}(P_o)$ decreases with P_o) so that heat transfer from the top regions of the bubble surface to the subcooled liquid should decrease (this same argument applies if P_o is fixed while T_∞ is increased as discussed below). With reduced heat loss, the bubble can remain at the surface for a longer period and the delay time should then increase. This trend is qualitatively consistent with Figs. 7 and 8. This same effect should occur if P_o is fixed (whereby T_{sat} is also fixed) and T_∞ is increased.

Fig. 9 shows the evolution of average surface temperature with T_∞ for $P_o = 0.101$ MPa and pulse times of 40 μs . As T_∞ increases the oscillation frequency decreases. This trend is consistent with progressively reduced heat loss from the bubble as T_∞ is increased for a fixed T_{sat} (since P_o is fixed for the results in Fig. 9) as noted above. At the highest T_∞ (93 °C) temperature oscillations completely disappear over the range of the pulse time examined as shown in Fig. 9. This result suggests a net heat input to the bubble over the duration of the heat pulse, as $T_{\text{sat}} - T_\infty$ is evidently too low to promote bubble collapse. At $T_\infty = 93 \text{ °C}$ the surface temperature increases in a manner consistent with the metal film being a lumped thermal system.

The trigger for the onset of temperature oscillations is unknown. A possible mechanism is that the macroscopic bubble or vapor film that covers the surface after nucleation during the waiting period is in a metastable state, balanced by heat input from the film and heat loss to the subcooled liquid. A small perturbation could upset this balance and initiate collapse after which a growth/decay cycle ensues that is manifested by temperature oscillations, assuming that the temperature tracks with the growth/collapse cycle.

The extent to which the surface temperature tracks with the bubble size was determined by simultaneously photographing

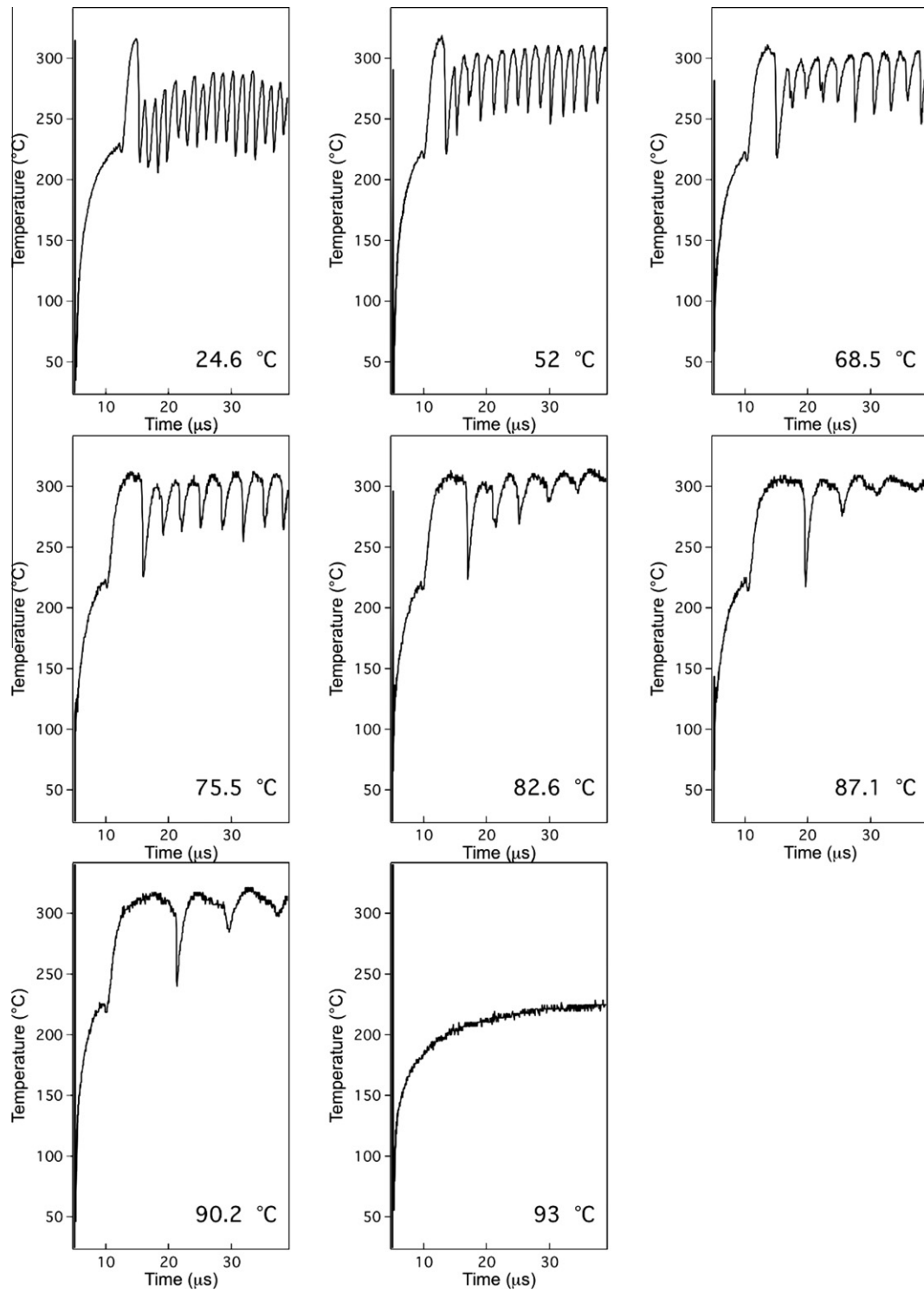


Fig. 9. Evolution of surface temperature for 40 μs pulse widths at various ambient temperatures, T_∞ for $P_0 = 0.101 \text{ MPa}$.

the surface of the film and recording the surface temperature during a constant heat input. The high speed imaging arrangement used for this purpose requires a fair degree of repeatability of bubble morphology at each instant of the growth/collapse cycle to establish a time sequence of the process from individual images taken at different times in the cycle. We show some results for ethanol boiling on a $AR = 6.6$ film. This smaller AR facilitated confining the bubble volume to the microscope field of view. A 50 μs voltage pulse was imposed on the films.

As shown in Fig. 10, the bubbles are not spherical during the “growth” and “collapse” phases though they do appear to start out as spherical bubbles (Fig. 10a, which is close to the inflection point). The critical size bubbles, with predicted radius of about 51 nm (at 200 $^\circ\text{C}$), would be too small to be photographed. The bubbles shown in Fig. 10 are well into the growth phase and $P \approx P_0$. As the bubbles grow, coalescence creates oblong structures (Fig. 10b and c) that loosely conform to the shape of the platinum film footprint. The collapse process (Fig. 10c–e) physically breaks

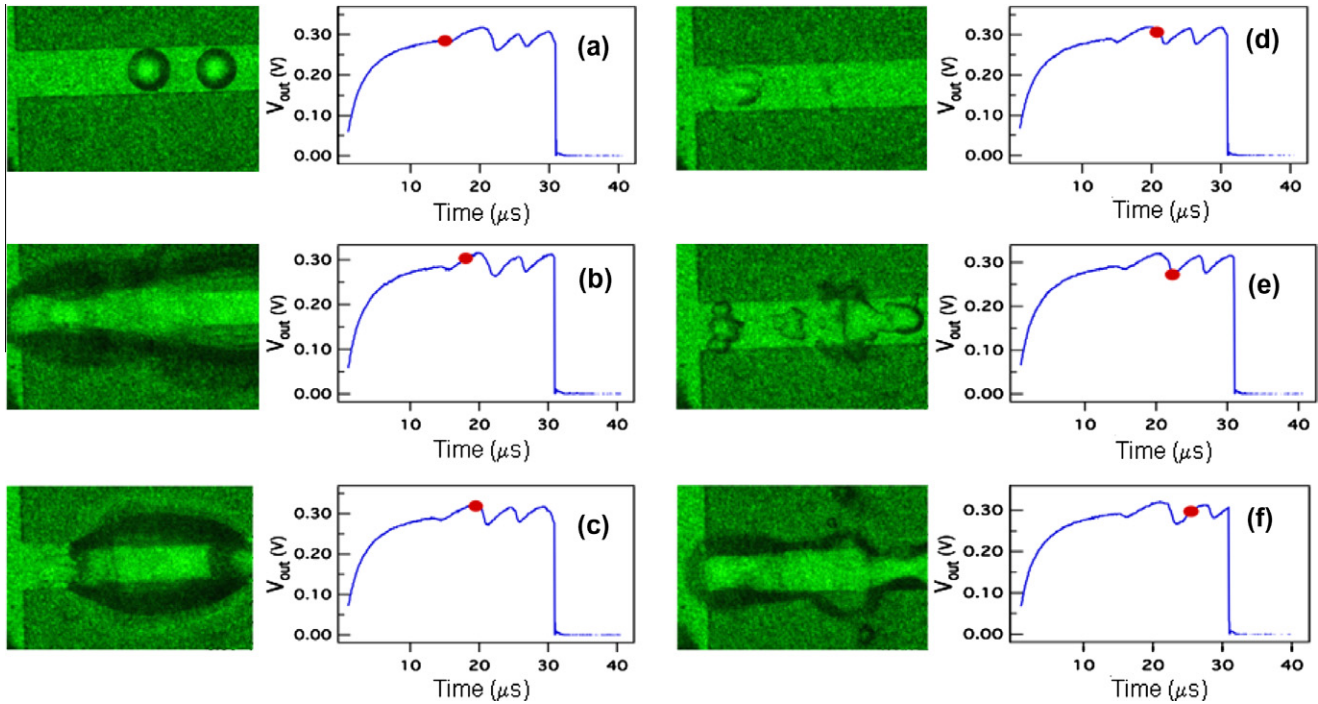


Fig. 10. Photographs of bubbles at various stages of one cycle of a growth and collapse sequence. The fluid is ethanol and the pulse duration is 30 μs. The photographs and V_{out} measurements were taken simultaneously. The “dots” placed on the voltage traces adjacent to each photograph correspond to the time of the laser flash that provided the illumination for the photograph. The total range of the voltage plot is 0.35 V for all six traces. The device was 7 μm × 46 μm with an aspect ratio AR = 6.6.

Table 1
Water property values (evaluated at 403 K).

σ (N/m)	ρ_L (kg/m ³)	ρ_v (kg/m ³)	C_{pL} (J/kg K)	C_{pv} (J/kg K)	h_{fg} (J/kg)	k_L (W/m K)	L_μ (kg/s m)
0.053	934	1.51	4266	2177	2.17×10^6	0.688	2.10×10^{-3}

up the elongated bubble into smaller bubbles (Fig. 10e), perhaps by a combination of surface tension and the physical dynamics of the collapse.

The evolution of V_{out} is shown adjacent to each image in Fig. 10. Because the AR = 6.6 heater was too small to promote a uniform surface temperature, no attempt was made to convert the V_{out} traces in Fig. 10 to temperature though we know that $T_w \propto V_{out}$. The voltage traces are essentially quasi-static in that repeated pulsing produced almost coincident traces. The red dot indicates the time when the adjacent photograph was taken in the growth/collapse cycle. In the growth phase (10b–10d) the temperature rises. After collapse where the single large bubble breaks up into smaller structures the surface temperature decreases from 10c to 10e. These trends show that the surface temperature does qualitatively track with the evolution of bubble size (Fig. 1b and c).

We know of no quantitative analysis to predict the trends noted above. Qualitative explanations for surface temperature oscillations during bubble growth and collapse in subcooled liquids [9,12,17,29,30] note the importance of energy loss at the upper regions of the bubble as it grows outside of the superheated liquid layer. During the growth phase the surface temperature increases as the surface is covered with vapor, and there is a net energy input to the bubble. When the bubble penetrates well into the subcooled liquid the bubble begins to lose energy and condensation occurs and the bubble size decreases causing an inflow of cold liquid to the surface that drops the temperature. Repeating this process results in temperature oscillations.

A quantitative explanation of temperature oscillations was obtained by considering a single temperature cycle as schematically shown in Fig. 1b and c. Conditions that would decrease the bubble lifetime t_b (i.e., the time from growth to collapse) should increase the oscillation frequency. Early bubble growth theories that included predictions of t_b incorporated an energy loss term to account for condensation of the bubble as it grew beyond the superheated liquid layer adjacent to the surface [30,31].

Few numerical studies related to bubble nucleation and growth at heated surfaces in subcooled liquids considered temperature

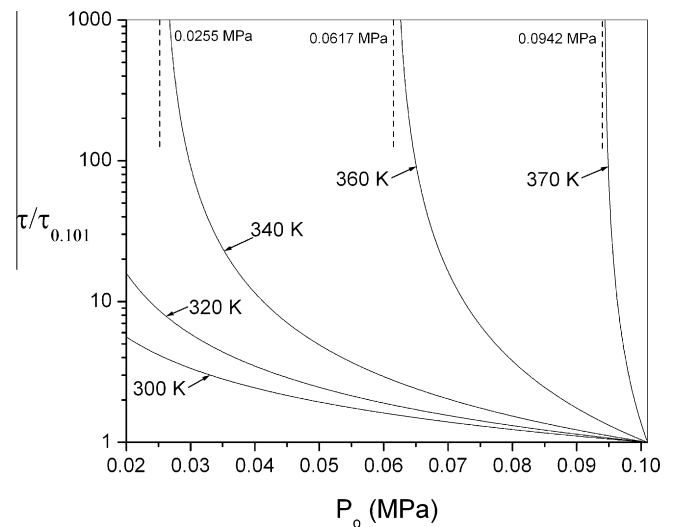


Fig. 11. Variation of computed nondimensional bubble growth/collapse time (from Eq. (7)), $\tau = t_b/t_w$, normalized by the nondimensional time ($\tau_{0.101}$) at $P_0 = 0.101$ MPa. The parameter is the bulk liquid temperature, T_∞ . Dotted lines indicate the saturation pressure corresponding to T_∞ at which the normalized growth/collapse time is infinite.

oscillations during growth/collapse cycles. Wu and Dhir [32] and Son et al. [33] computed flow patterns around bubbles growing from surfaces into subcooled liquids and showed departure cycles with oscillating Nusselt numbers. Algorithms have also been developed for tracking the detailed shape of bubbles formed in film boiling on superheated surfaces that included the flow dynamics around the growing and departing bubbles [34,35]. Of the many analytical theories that have been developed for bubble growth and collapse, the one by Mikic and Rohsenow [31] offers a relatively simple analytical approach to understanding the trends of the data. This, and similar models [30,36], may be considered to predict the growth/collapse history of a single cycle of an oscillation (Fig. 1b and c). The simplifying assumptions in the model include one-dimensional transport, constant properties, thermally controlled growth, hemispherical bubble, and neglect of surface tension and liquid inertia.

An energy balance on the bubble results in an analytical expression for the evolution of bubble radius as

$$R = \frac{2}{\pi} \sqrt{3} Ja \sqrt{\pi \alpha t} \left[1 - \Theta \left\{ \left(1 + \frac{1}{(t/t_w)} \right)^{1/2} - \frac{1}{(t/t_w)^{1/2}} \right\} \right] \quad (7)$$

where

$$Ja = \frac{(T_w - T_{sat}) c_{pl} \rho_L}{h_{fg} \rho_v} \quad (8)$$

$$\Theta = \frac{T_w - T_\infty}{T_w - T_{sat}(P_o)} \quad (9)$$

and t_w is the time at which the liquid reaches the nucleation temperature at a distance r from the surface. There are two roots for $R = 0$ (term in brackets) for Eq. (7): one at $t = 0$ (the initial condition) and another at $t = t_b$. Eq. (7) is used to infer how $\tau \equiv t_b/t_w$ varies with parameters to explain bubble, and hence surface temperature, oscillations. Property values were fixed for all conditions since the theory assumes constant properties. The properties used are listed in Table 1.

Fig. 11 shows the predicted variation of $\tau/\tau_{0.101}$ (i.e., relative to the bubble growth time for $P_o = 0.101$ MPa) with P_o for the indicated T_∞ . The asymptotes are the saturation pressures corresponding to T_∞ at which state the computed collapse times are infinite (i.e., the bubble does not collapse). The results show that as P_o decreases the relative bubble growth time increases. Since the surface temperature qualitatively tracks with the growth and collapse cycle (Fig. 10), an increasing $\tau/\tau_{0.101}$ implies a decreasing temperature oscillation frequency which is consistent with the data in Figs. 7 and 8. Similarly, for a fixed P_o Fig. 11 also shows that the bubble collapse time (t_b or $\tau/\tau_{0.101}$) increases with T_∞ . By inference, a longer collapse time would correspond to a smaller frequency. This trend is also consistent with Fig. 9.

4. Conclusions

The bubble nucleation temperature is unaffected by pressure in the sub-atmospheric range examined because the internal bubble (vapor) pressure is much greater than the surrounding liquid pressure over the ambient pressure range examined. However, ambient pressure affects the temperature difference driving energy exchange between the bubble and surrounding liquid which in turn influences temperature oscillations. Surface temperature oscillations occur at frequencies that decrease with decreasing subcooling, and increase with increasing pressure. The trends follow qualitative expectations from thermally controlled bubble growth theories that incorporate a heat loss mechanism to the subcooled liquid.

A strong effect of nucleation temperature on heating rate was observed. At low rates ($<10^6$ °C/s) the nucleation temperature is constant suggesting the presence of gas pockets of a fixed size that are trapped during the liquid spreading process and the temperature levels off at 200°C. For heating rates above this temperature, the nucleation temperature increases approximately linearly with heating rate until the homogenous nucleation temperature (290 °C) is reached at a heating rate of about 10^9 °C/s. High-speed imaging shows that the evolution of bubble morphology qualitatively tracks with surface temperature in the cyclic temperature history.

Acknowledgements

The authors are pleased to acknowledge the expertise of Mr. Michael Carrier of the National Institute of Standards and Technology (Gaithersburg, MD) to fabricate the AR=10 devices. Discussions with Dr. Michael Tarlov of NIST are greatly appreciated.

References

- [1] J.H. Lienhard IV, J.H. Lienhard V, A Heat Transfer Textbook, third ed., Plhlogiston Press, Cambridge, MA, 2003. pp. 465, 472.
- [2] R.R. Allen, J.D. Meyer, W.R. Knight, Thermodynamics and hydrodynamics of thermal ink jets, Hewlett-Packard J. 36 (1985) 21–27.
- [3] T. Kraemer, Printing enters the jet age, Invent Technol. 16 (2001) 18–27.
- [4] M. Staples, K. Daniel, M.J. Cima, R. Langer, Application of micro and nano electromechanical devices to drug delivery, Pharmaceut. Res. 23 (2006) 847–863.
- [5] D.J. Laser, J.G. Santiago, A review of micropumps, J. Micromech. Microeng. 14 (2004) R35–R64.
- [6] X. Geng, H. Yuan, H.N. Oguz, A. Prosperetti, Bubble-based micropump for electrically conducting liquids, J. Micromech. Microeng. 11 (2001) 270–276.
- [7] T. Chen, J.F. Klausner, J.N. Chung, Subcooled boiling heat transfer and dryout on a constant temperature microheater, Int. J. Heat Fluid Flow 25 (2004) 274–287.
- [8] J. Kim, C. Henry, Heater Size and Gravity Effects on Pool Boiling Heat Transfer, CP654, in: M.S. El-Geng (Ed.), Space Technology and Applications International Forum – STAIF 2003, American Institute of Physics.
- [9] C.T. Avedisian, W.S. Osborne, F.D. McLeod, C.M. Curley, Measuring bubble nucleation temperature on the surface of a rapidly heated thermal ink-jet heater immersed in a pool of water, Proc. Roy. Soc. London Ser. – Math. Phys. Eng. Sci. 455 (1999) 3875–3899.
- [10] C.T. Avedisian, The thermal ink jet printer: a paradigm for microscale phase change, in: Proceedings of 5th ISHMT-ASME Heat and Mass Transfer Conference and 16th National Heat Transfer Conference, Tata McGraw-Hill, Calcutta, 2002, ISBN 0-07-047443-5. pp. 169–175.
- [11] S.A. Zhukov, V.A. Rafeev, S. Yu, S.B. Afans'ev, S.B. Echmaev, B.L. Korsunksii, Singularities of realization of film boiling on wire heaters, High Temp. 41 (2003) 243–251.
- [12] G. Romera-Guereca, T.Y. Choi, D. Poulikakos, Explosive vaporization and microbubble oscillations on submicron width thin film strip heaters, Int. J. Heat Mass Transfer 51 (2008) 4427–4438.
- [13] C.T. Avedisian, R.E. Cavicchi, M.J. Tarlov, New technique for visualizing microboiling phenomena and its application to water pulse heated by a thin metal film, Rev. Sci. Instrum. 77 (2006) 063706.
- [14] O.C. Thomas, R.E. Cavicchi, M.J. Tarlov, Effect of surface Wettability on fast transient microboiling behavior, Langmuir 19 (2003) 6168–6177.
- [15] R.E. Cavicchi, C.T. Avedisian, Bubble nucleation and growth anomaly for a hydrophilic microheater attributed to metastable nanobubbles, Phys. Rev. Lett. 98 (2007) 124501.
- [16] K.M. Balss, C.T. Avedisian, R.E. Cavicchi, M.J. Tarlov, Imaging microboiling behavior on pulsed heated Au films modified with hydrophilic and hydrophobic self-assembled monolayers, Langmuir 21 (2005) 10459–10467.
- [17] H.S. Lee, H. Merte, The origin of the dynamic growth of vapor bubbles related to vapor explosions, J. Heat Transfer 120 (1998) 174–182.
- [18] C.T. Avedisian, The homogeneous nucleation limits of liquids, J. Phys. Chem. Ref. Data 14 (1985) 695–720.
- [19] J. Li, G.P. Peterson, Boiling nucleation and two-phase flow patterns in forced liquid flow in microchannels, Int. J. Heat Mass Transfer 48 (2005) 4797–4810.
- [20] R.F. Apfel, Vapor Cavity Formation in Liquids, Technical Memorandum #62, Acoustics Research Laboratory, Harvard Univ., Cambridge, 1970.
- [21] A.W. Adamson, A.P. Gast, Physical Chemistry of Surfaces, sixth ed., Wiley, Berlin, 1997. pp. 365–366.
- [22] J.J. Lorenz, B.B. Mikic, W.M. Rohsenow, The Effect of Surface Conditions on Boiling Characteristics, Report No. DSR 73413-79, Department of Mechanical Engineering, Engineering Projects Laboratory, Massachusetts Institute of Technology, Cambridge, December 1972 (also Proc. 5th Int. Heat Transf. Conf., vol. 5, Hemisphere, New York, 1974).
- [23] J. Li, P. Cheng, Bubble cavitation in a microchannel, Int. J. Heat Mass Transfer 47 (2004) 2689–2698.

- [24] R.C. Tolman, The effect of drop size on surface tension, *J. Chem. Phys.* 17 (1949) 333–337.
- [25] L.S. Bartell, Tolman's δ surface curvature compressibility effects and the free energy of drops, *J. Phys. Chem. B* 105 (2001) 11615–11618.
- [26] F.P. Incropera, D.P. DeWitt, *Introduction to Heat Transfer*, fourth ed., John Wiley & Sons, New York, 2002.
- [27] C.T. Avedisian, Bubble Growth in Superheated Liquid Droplets, *Encyclopedia of Fluid Mechanics*, Gulf Publ. Co., Houston, 1986, pp. 130–190 (Chapter 8).
- [28] A. Prosperetti, M. Plesset, Vapour-bubble growth in a superheated liquid, *J. Fluid Mech.* 85 (1978) 349–368.
- [29] F.D. Moore, R.B. Mesler, The measurement of rapid surface temperature fluctuations during nucleate boiling of water, *AIChE J.* 7 (1961) 620–624.
- [30] N. Zuber, The dynamics of vapor bubbles in nonuniform temperature fields, *Int. J. Heat Mass Transfer* 2 (1961) 83–98.
- [31] B.B. Mikic, W.M. Rohsenow, Bubble growth rates in non-uniform temperature field, *Prog. Heat Mass Transfer* 2 (1969) 284–292.
- [32] J. Wu, V.K. Dhir, Numerical simulations of the dynamics and heat transfer associated with a single bubble in subcooled pool boiling, *J. Heat Transfer* 132 (2010) 111501.
- [33] G. Son, V.K. Dhir, N. Ramanujapu, Dynamics and heat transfer associated with a single bubble during nucleate boiling on a horizontal surface, *J. Heat Transfer* 121 (1999) 623–631.
- [34] A. Esmaeeli, G. Tryggvason, Computations of film boiling Part I: numerical method, *Int. J. Heat Mass Transfer* 47 (2004) 5451–5461.
- [35] D. Banerjee, V.K. Dhir, Study of subcooled film boiling on a horizontal disc: Part 2 – Experiments, *J. Heat Transfer* 123 (2001) 285–293.
- [36] K. Nishikawa, H. Kusuda, K. Yamasaki, Growth and collapse of bubbles in nucleate boiling, *Bull. JSME* 8 (1965) 205–210.